Mechanisms underlying homeostatic plasticity in the *Drosophila* mushroom body in vivo

Anthi A. Apostolopoulou[a,b] and Andrew C. Lin[a,b,1]

[a]Department of Biomedical Science, University of Sheffield, Sheffield S10 2TN, United Kingdom; and [b]Neuroscience Institute, University of Sheffield, Sheffield S10 2TN, United Kingdom

Edited by Liqun Luo, Stanford University, Stanford, CA, and approved May 27, 2020 (received for review December 6, 2019)

Neural network function requires an appropriate balance of excitation and inhibition to be maintained by homeostatic plasticity. However, little is known about homeostatic mechanisms in the intact central brain in vivo. Here, we study homeostatic plasticity in the *Drosophila* mushroom body, where Kenyon cells receive feedforward excitation from olfactory projection neurons and feedback inhibition from the anterior paired lateral neuron (APL). We show that prolonged (4-d) artificial activation of the inhibitory APL causes increased Kenyon cell odor responses after the artificial inhibition is removed, suggesting that the mushroom body compensates for excess inhibition. In contrast, there is little compensation for lack of inhibition (blockade of APL). The compensation occurs through a combination of increased excitation of Kenyon cells and decreased activation of APL, with differing relative contributions for different Kenyon cell subtypes. Our findings establish the fly mushroom body as a model for homeostatic plasticity in vivo.

Drosophila | olfaction | homeostatic plasticity | mushroom body

Effective information coding in neural networks requires neuronal firing rates to stay within a certain dynamic range. At the extremes, networks carry no useful information if neurons are completely silent or constantly fire at their highest possible rate. More subtle differences in activity levels can also affect information coding; for example, sparse coding of sensory stimuli helps to maximize associative memory capacity and to separate population representations of different stimuli, thereby enhancing learned discrimination (1, 2). Yet how do neural networks achieve such "Goldilocks" activity levels, and how do they maintain them in the face of external perturbations (e.g., temperature changes) or neural plasticity caused by development or learning (e.g., Hebbian plasticity, which risks destabilizing activity levels by strengthening active synapses and weakening inactive synapses)? Theoretical studies show that this problem can be solved by homeostatic plasticity, which compensates for changes in activity levels to restore neurons to a "set point" of activity (3, 4). Such homeostatic plasticity can occur through multiple mechanisms, including changes in intrinsic excitability, strength or number of excitatory or inhibitory synaptic inputs, or changes in the threshold between synaptic potentiation vs. depression (5, 6).

These findings have mostly come from dissociated neurons in vitro or ex vivo preparations like brain slices, sometimes following in vivo sensory deprivation like eyelid suture (e.g., refs. 7–13). Yet brain slices differ in important ways from the intact brain in vivo: Compared with the intact brain, brain slices can have less spontaneous activity (14) and more synapses (15). Even in vivo, neural activity differs significantly between awake and anesthetized animals (16). Homeostatic compensation has been studied in vivo in the spinal cord (17, 18) and more recently in the brain (19–24), but the circuit mechanisms underlying homeostatic plasticity in the intact central brain in vivo remain relatively unknown.

This problem can be addressed in *Drosophila*, whose genetic toolkit and numerically simple brain allow greater specificity in manipulating and measuring neural activity in vivo than in mammals. These tools have revealed many examples at cellular resolution of plasticity underlying associative learning (25), nonassociative learning (26–28), activity-dependent remodeling (29, 30), and developmental circuit refinement (31). However, relatively little is known about homeostatic regulation of activity levels (but see, e.g., ref. 32). In most examples of homeostatic compensation studied in *Drosophila*, the variable being controlled is not activity level but synaptic strength. In particular, in the most well understood homeostatically controlled system, the neuromuscular junction, the goal is to maintain constant synaptic strength so that the muscle can faithfully execute the motor neuron's commands, not to maintain constant average activity levels in the muscle (33) (see also ref. 34 for the antennal lobe). It remains unclear whether or how the adult fly brain uses homeostatic plasticity to maintain activity levels in the correct range.

We address this question in the fly mushroom body, whose principal neurons, called Kenyon cells (KCs), receive both feedforward excitation from second-order olfactory neurons called projection neurons (PNs) and feedback inhibition from a single neuron called "APL" (anterior paired lateral; Fig. 1*A*) (1, 35–37). This balance of excitation and inhibition regulates the level of activity in KCs to enforce sparse coding, in which only a small fraction of KCs responds to each odor (38). This sparse coding reduces overlap between KC odor representations and enhances learned odor discrimination (1). However, it remains unclear how KCs set the relative strengths of their excitatory and inhibitory inputs. We hypothesized that this balance might be set in an activity-dependent manner, in which case the mushroom

Significance

When a neuron fires, it excites or inhibits other neurons. These two opposing forces—excitation and inhibition—need to be carefully balanced in the brain for neural networks to function properly. Maintaining this balance requires homeostatic plasticity to compensate for perturbations in neural activity levels. Relatively little is known about how such homeostatic compensation works in the intact central brain in vivo. To address this problem, we developed a model for studying homeostatic plasticity in vivo: the *Drosophila* mushroom body (the fly's olfactory memory center). We found that this brain structure compensates for prolonged excess inhibition through a combination of increased excitation and decreased inhibition, with these two mechanisms contributing differently for different types of neurons.

Author contributions: A.A.A. and A.C.L. designed research, performed research, contributed new reagents/analytic tools, analyzed data, and wrote the paper.

The authors declare no competing interest.

This article is a PNAS Direct Submission.

Data deposition: Analysis code is available on GitHub at https://github.com/aclinlab/calcium-imaging.

[1]To whom correspondence may be addressed. Email: andrew.lin@sheffield.ac.uk.

This article contains supporting information online at https://www.pnas.org/lookup/suppl/doi:10.1073/pnas.1921294117/-/DCSupplemental.

First published June 29, 2020.

body should homeostatically adapt to perturbations in activity levels.

Here we test the homeostatic capacity of the fly mushroom body in vivo and dissect the underlying circuit mechanisms. We find that the mushroom body compensates for excess inhibition from APL but shows little compensation for lack of inhibition. Compensation for excess inhibition from APL requires multiple days and occurs by both weakening odor-evoked activity of APL and increasing odor-evoked excitation of KCs, with differing relative contributions of these two mechanisms in different subtypes of KCs. These findings establish the fly mushroom body as a model for studying homeostatic plasticity in vivo.

Results

KCs Show Little Compensation for Loss of Inhibition from APL. We first tested whether the mushroom body circuitry adapts to lack of inhibition from APL. Previously, we showed that blocking synaptic output from APL by acutely expressing tetanus toxin (TNT) in APL dramatically increases odor-evoked Ca^{2+} influx in KCs (1, 39). We now compared the effects of blocking inhibition from APL acutely (16 to 24 h) vs. constitutively (throughout development) (Fig. 1*B*). As before, we expressed TNT in APL by intersecting the expression domains of NP2631-GAL4 and GH146-FLP, suppressing GAL4 activity in GH146-negative cells by including tubP-FRT-GAL80-FRT. GAL80 is excised in GH146-positive cells by FLP recombinase ~50 to 70% of the time (1). This method drives expression of UAS transgenes in APL and not in PNs or KCs (1) (*SI Appendix*, Fig. S1 *A* and *B*). To express TNT acutely, we included tubP-GAL80^{ts} to suppress GAL4 activity when flies were kept at 18 °C, and induced expression of TNT by heating the flies to 31 °C for 16 to 24 h before the experiment. To express TNT in APL constitutively, we left out the tubP-GAL80^{ts} but exposed the flies to the same temperatures as the "acute" flies (Fig. 1*B*).

To confirm that tubP-GAL80^{ts} effectively suppressed GAL4 activity in APL in acute flies, we drove expression of green fluorescent protein (GFP) and mCherry in APL (see *SI Appendix*, Table S1 for full genotypes). These flies showed GFP expression in APL in 12/18 hemispheres when raised at 18 °C and heated to 31 °C for 16 to 24 h before dissection [consistent with previous studies (1)] but in 0/15 hemispheres when kept at 18 °C. Given that both conditions have the same probability of GAL80 excision [excision occurs in development (40), so would be unaffected by heating during adulthood], it is extremely unlikely that GAL80 would be excised in APL in 12/18 hemispheres in one condition but 0/15 in the other ($P < 0.0001$, Fisher's exact test). Thus, the most plausible explanation is that GAL80 was excised in APL even in the flies kept at 18 °C but GAL4 activity was effectively suppressed by tubP-GAL80^{ts}.

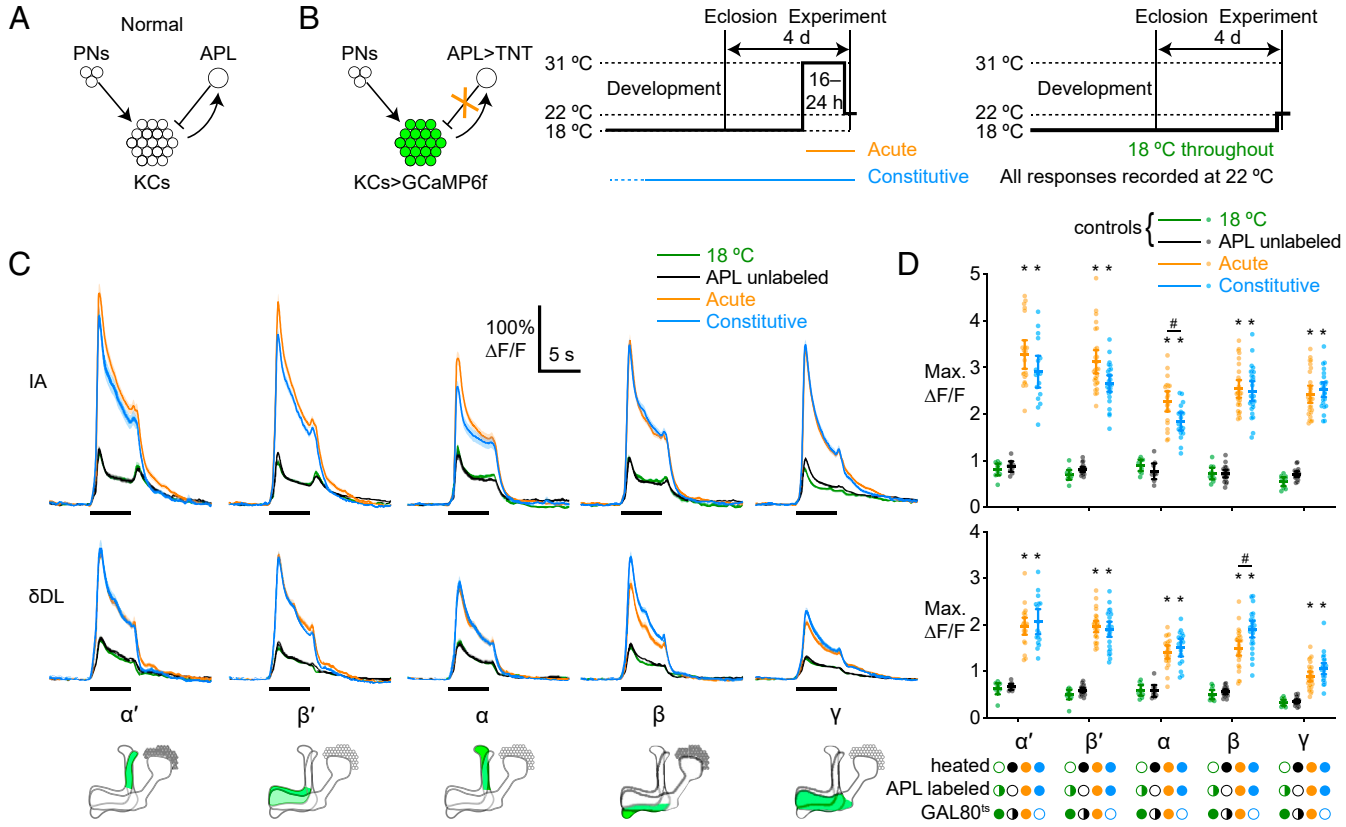

Fig. 1. Kenyon cells show little compensation for loss of inhibition from APL. (*A*) Schematic of mushroom body circuitry. Kenyon cells receive feedforward excitation from projection neurons and feedback inhibition from APL. (*B*) Diagram of genotype (green shows GCaMP6f expression; the orange "X" shows blockade with TNT) and experimental protocol. Flies were raised at 18 °C, collected 0 to 1 d after eclosion, and then kept at 18 °C for 3 d and heated to 31 °C for 16 to 24 h (*Center*) or kept at 18 °C for 4 d (*Right*) before the imaging experiment, which was always done at 22 °C. (*C*) Responses of different KC lobes to isoamyl acetate (IA; *Top*) or δ-decalactone (δDL; *Middle*), imaged with GCaMP6f. Black bars indicate 5-s odor pulse; shading indicates SEM. (*C*, *Bottom*) Diagrams show the locations of different lobes in the mushroom body (green; medial is left, and dorsal is up). See also *SI Appendix*, Figs. S2 and S3. (*D*) Maximum Δ*F*/*F* of data from *C*. Half-filled circles indicate the category pooled data, that is, APL labeled and unlabeled (green), with GAL80^{ts} and without (black). Mean ± 95% CIs. $^{\#}P < 0.05$ between acute vs. constitutive; $^{*}P < 0.001$ between TNT expressed (acute or constitutive) vs. TNT not expressed (18 °C or APL unlabeled), ANOVA (see *SI Appendix*, Table S2 for details). *n*, given as the number of hemispheres (number of flies), left to right: α′ and α, 9 (5), 9 (7), 22 (15), 17 (10); β′, β, and γ, 10 (5), 19 (14), 28 (19), 26 (15).

To measure KC odor responses, we expressed GCaMP6f in KCs under the control of MB247-LexA (41), and TNT in APL, using the above-described intersectional strategy. MB247-LexA does not drive expression in APL (1) (*SI Appendix*, Fig. S1 *C* and *D*). To test KC responses for different strengths of excitatory input, we recorded Ca^{2+} influx in KCs evoked by the "strong" odor isoamyl acetate and the "weak" odor δ-decalactone [the former elicits more total activity in olfactory receptor neurons (42) and KCs (1)]. We separately analyzed KC odor responses in the different lobes of the mushroom body, namely the α′ and β′ lobes (made up of axons from α′β′ KCs), α and β lobes (axons from αβ KCs), and γ lobe (axons from γ KCs) (see diagrams in Fig. 1*C*), because the three main KC subtypes (α′β′, αβ, and γ) have different functional properties (43–46).

We used two negative controls in which APL did not express TNT. First, we measured KC odor responses in brain hemispheres in which GAL80 was not excised in APL (i.e., identical genotype and treatment but no TNT in APL: "APL unlabeled," black in Fig. 1 *C* and *D*). We identified which hemispheres had GAL4 activity in APL by including UAS-mCherry or immunostaining brains for TNT after the experiment. (We pooled the APL unlabeled hemispheres from flies with and without tubP-GAL80^{ts} because their odor responses did not differ [*SI Appendix*, Fig. S2*A*]; conclusions from the statistical analysis are unchanged if the two groups are separated [*SI Appendix*, Table S2].)

Second, to further confirm that tubP-GAL80^{ts} suppressed TNT expression in APL to functionally insignificant levels, we measured KC odor responses in flies with tubP-GAL80^{ts} that were kept at 18 °C throughout life (diagram in Fig. 1 *B*, *Right*; data labeled "18 °C", green in Fig. 1 *C* and *D*). These flies showed similar responses as the APL unlabeled controls. Although we could not confirm whether GAL80 had been excised from tubP-FRT-GAL80-FRT in APL in these flies (due to the continued activity of GAL80^{ts}), it is unlikely that all 18 °C flies would have had APL unlabeled by chance, given that 28/40 hemispheres had APL labeled in the corresponding experimental flies that were heated to 31 °C (0/10 at 18 °C vs. 28/40 at 31 °C, $P < 0.0001$, Fisher's exact test), by the same logic as the GFP expression experiment above. This second negative control confirms that our acute expression of TNT was genuinely acute, with functionally no leaky expression of TNT during development.

Compared with both of these control groups, both acute and constitutive expression of TNT in APL dramatically increased odor-evoked Ca^{2+} influx in KCs (Fig. 1 *C* and *D*), with little evidence of homeostatic compensation. We did not observe any consistent differences in KC response amplitudes between acute vs. constitutive APL>TNT flies. In some cases, constitutive responses were lower than acute responses and, in others, they were higher (KC responses are imaged with GCaMP6f in Fig. 1 and GCaMP3 in *SI Appendix*, Fig. S2*B*). Other subtle differences occasionally appeared, for example, a smaller normalized difference between responses to isoamyl acetate and δ-decalactone in constitutive APL>TNT flies, potentially suggesting compensation to restore APL's gain control function, or reduced post-odor GCaMP signal in constitutive APL>TNT flies, potentially suggesting altered calcium export (*SI Appendix*, Fig. S3). However, again, these differences were subtle and inconsistent, and thus do not provide clear evidence of functionally significant adaptation. Thus, taken together, our data indicate that Kenyon cells show little, if any, homeostatic compensation for prolonged lack of inhibition from APL.

KC Odor Responses Are Higher following Prolonged Excess Inhibition from APL. We next tested the reverse manipulation: Rather than blocking APL, we activated APL with the temperature-sensitive cation channel dTRPA1 (47). Acutely activating APL with dTRPA1 suppresses odor responses in KCs (1) and activation with dTRPA1 throughout development induces homeostatic plasticity in larval motor neurons (29). Given that mammalian cortical plasticity induced by sensory deprivation can take several days to appear (24, 48), we initially activated APL for 4 d. We expressed GCaMP6f in KCs and dTRPA1 and mCherry in APL, using the same drivers as in Fig. 1. We raised flies at 22 °C, collected them 0 to 1 d after eclosion, and either left them at 22 °C or heated them to 31 °C for 4 d (88 to 96 h) before recording KC odor responses at 22 °C (Fig. 2*A*).

If this prolonged artificial activation of APL induces homeostatic compensation, KC activity should rebound to abnormally high levels when the artificial activation is stopped. Indeed, KC odor responses recorded at 22 °C were significantly higher in hemispheres where APL expressed dTRPA1 when the flies had been preheated to 31 °C for 4 d, compared with hemispheres where APL was unlabeled or with flies that had not been preheated. This effect occurred in all lobes, with both the strong odor isoamyl acetate and the weak odor δ-decalactone (Fig. 2 *B* and *C*). Similar effects were seen when measuring odor responses with GCaMP3 instead of GCaMP6f (*SI Appendix*, Fig. S4), although the effect in α′β′ KCs was less consistent here and in later experiments (see below). Note that "APL unlabeled" and "APL>dTRPA1" hemispheres had the same genotype and in many cases were in the same fly, providing an ideal genetic control.

Increased responses in KC axonal lobes could reflect individual KCs responding more and/or more KCs responding. To test the latter possibility, we recorded KC somatic odor responses in preheated flies and measured the population sparseness of the resulting activity maps. Odor responses were less sparse (broader) in APL>dTRPA1 hemispheres compared with APL unlabeled hemispheres (Fig. 2 *D* and *E* and *SI Appendix*, Fig. S5*A*). We next asked if this broadening would also make KC odor responses more similar. Although interodor correlations between activity maps were somewhat higher in APL>dTRPA1 hemispheres, the effect was not statistically significant (*SI Appendix*, Fig. S5 *B* and *C*). We may lack statistical power to detect a modest effect, but our sample size provided 96% power to detect an effect as large as the increase in interodor correlations previously observed in APL>TNT flies (1). This difference could be explained by the fact that adaptation to APL activation causes a much smaller increase in KC odor responses than APL>TNT does (*SI Appendix*, Fig. S5*D*).

The smaller effect of adaptation to APL>dTRPA1 (vs. blocking APL with TNT) also implies that the adaptation effect cannot be explained trivially as APL simply being killed or damaged by overactivation by dTRPA1 for 4 d. This trivial explanation is further excluded by the fact that even after we preactivated APL with dTRPA1, heating flies to 31 °C during the imaging experiment to acutely activate APL still efficiently suppressed KC odor responses (*SI Appendix*, Figs. S6 and S7; see also Fig. 5 below). Moreover, adaptation to APL>dTRPA1 caused no obvious changes in the gross morphology of KCs or APL (*SI Appendix*, Fig. S8). Together, these results suggest that 4-d APL>dTRPA1 activation induces homeostatic compensation to counteract the excess activity in APL or insufficient activity in Kenyon cells.

Adaptation to Excess Inhibition from APL Is Most Prominent after 4 d and Is Temporary. To further confirm these results, we repeated the APL>dTRPA1 adaptation experiments using a different APL driver, VT43924-GAL4, to express dTRPA1 in APL (49) (see *SI Appendix*, Fig. S1 *E–H* for the expression pattern). Kenyon cells' odor responses recorded after a 4-d preactivation of APL were significantly higher (except in the α′ lobe) in flies where APL expressed dTRPA1, compared with flies with UAS-dTRPA1 alone (Fig. 3*A*, blue squares, and *SI Appendix*, Fig. S9), thereby reproducing the results obtained with the intersectional strategy for labeling APL.

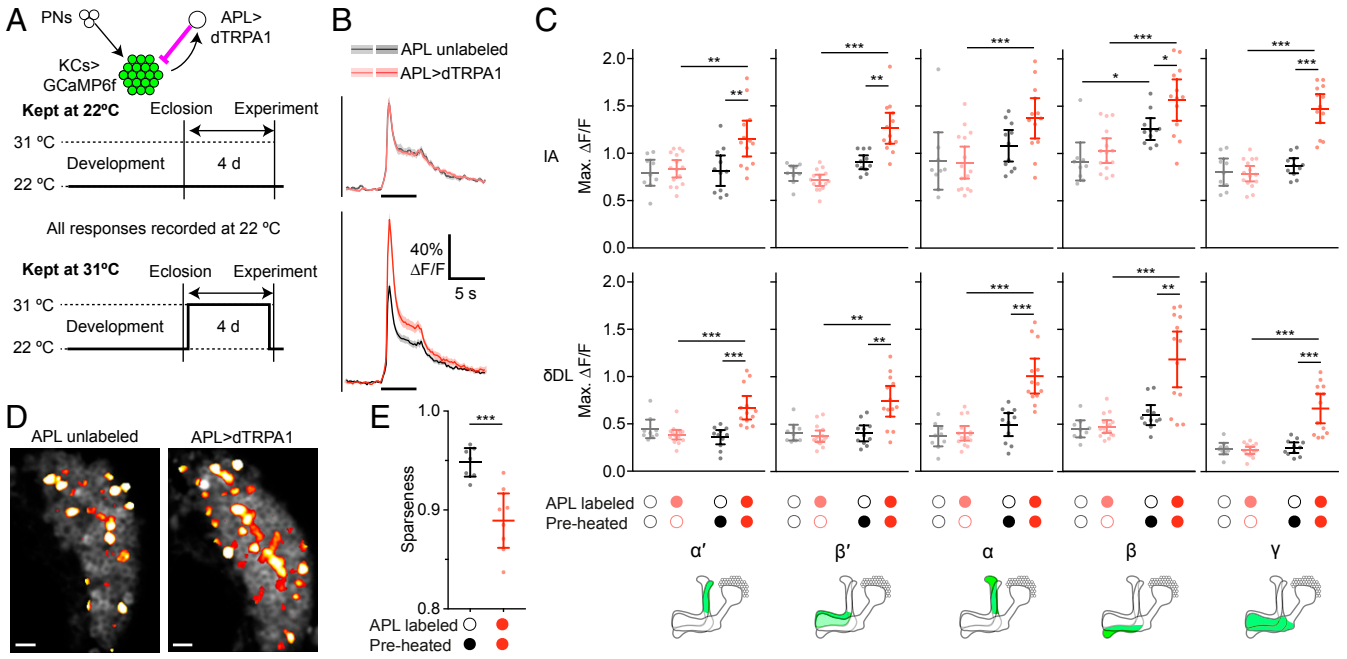

Fig. 2. Kenyon cell odor responses are higher following prolonged excess inhibition from APL. (*A*) Diagram of genotype (green shows GCaMP6f expression; magenta shows activation with dTRPA1) and experimental protocol. Flies were raised at 22 °C, collected 0 to 1 d after eclosion, kept at 22 °C (control) or 31 °C (preheated) for 4 d, and returned to 22 °C for the imaging experiment. (*B*) Responses of the γ lobe to isoamyl acetate, for flies kept at 22 °C (*Upper*) or 31 °C (*Lower*), where APL was unlabeled (gray/black) or expressed dTRPA1 (pink/red). Black bars indicate 5-s odor pulse; shading indicates SEM. Responses of all lobes are shown in *SI Appendix*, Fig. S4. (*C*) Maximum Δ*F*/*F* of odor responses in all lobes to isoamyl acetate and δ-decalactone. $*P < 0.05$, $**P < 0.01$, $***P < 0.001$, ANOVA (see *SI Appendix*, Table S2 for details). *n*, given as the number of hemispheres (number of flies), left to right within each graph: 9 (8), 15 (11), 11 (7), 13 (8). (*D*) Activity maps of responses to isoamyl acetate in KC somata. Grayscale shows baseline fluorescence of GCaMP6f; false-color overlay shows odor-responsive pixels. (Scale bars, 10 μm.) (*E*) Average sparseness to a panel of six odors (δ-decalactone, isoamyl acetate, ethyl butyrate, methylcyclohexanol, 3-octanol, and benzaldehyde; sparseness to each odor is shown separately in *SI Appendix*, Fig. S5). Mean ± 95% CIs. $***P < 0.001$, unpaired *t* test.

Other model systems show homeostatic compensation in as little as 1 d (9, 19, 23, 50–52). To test whether the mushroom body might similarly compensate within 1 d, we tested flies after 1 d of preactivating APL instead of 4 d, while still imaging them 4 to 5 d after eclosion (Fig. 3, blue squares, and *SI Appendix*, Fig. S9). Unlike with 4-d preheating, with 1-d preheating, APL>dTRPA1 flies did not have significantly higher KC odor responses than flies with UAS-dTRPA1 alone (although in some case there was a nonsignificant trend toward an increase).

This difference might arise not from the length of preheating but rather from the timing during the fly's life: Perhaps there is a critical period for homeostatic plasticity in the first day after eclosion. To test this, we preheated newly eclosed flies for 1 d. These flies also showed no significant difference between APL>dTRPA1 flies and UAS-dTRPA1 controls (*SI Appendix*, Fig. S10), suggesting that the difference between 1- and 4-d preheating is not due to a critical period (although there may still be a critical period such that, e.g., 10-d-old flies would not show homeostatic plasticity).

To further probe when compensation occurs, we tested flies at multiple time points: 1, 2, 3, and 4 d of heating (keeping the age of the fly at imaging constant). To reproduce our timescale results with a different driver, we returned to the NP2631/GH146-FLP intersectional driver (Fig. 3, black circles). Consistent with the results with VT43294-GAL4, only at 4 d did we consistently observe significantly higher KC odor responses in APL>dTRPA1 hemispheres compared with control APL unlabeled hemispheres (although at 1 to 3 d there was a trend toward an increase that was sometimes significant at 2 to 3 d; Fig. 3*A* and *SI Appendix*, Fig. S11). Here and in *SI Appendix*, Fig. S9, we do not exclude the possibility that some small adaptation occurs before 4 d that could not be detected with our statistical power, but these results suggest that the effect is more prominent after 4 d.

We next tested how long homeostatic compensation lasts, by taking flies where APL had been activated for 4 d and leaving them at 22 °C for 1, 2, or 3 d to "forget" the adaptation. The difference between APL>dTRPA1 and control hemispheres was no longer statistically significant by 1 to 2 d (Fig. 3*B* and *SI Appendix*, Fig. S12), suggesting that adaptation does not last more than 1 to 2 d after excess inhibition from APL stops.

APL Odor Responses Are Reduced following Adaptation. We next asked what cellular or circuit mechanisms underlie the adaptation observed above, namely increased odor responses in KCs following excess inhibition from APL. We postulated five broad, non-mutually exclusive categories of mechanisms: 1) increased synaptic excitation from PNs to KCs, 2) increased intrinsic excitability of KCs, 3) decreased synaptic excitation from KCs to APL, 4) decreased intrinsic excitability of APL, and 5) decreased synaptic inhibition from APL to KCs (Fig. 4*A*). Mechanisms 1, 2, and 5 center on KC activity while mechanisms 3 and 4 center on APL activity. To test these two broad groupings of hypotheses, we recorded odor responses in APL after adaptation (Fig. 4*B*). If adaptation only involves changes centered on KC activity (mechanisms 1, 2, and 5), then the relation between KC activity and APL activity would be unchanged; therefore, because APL's odor input comes from KCs (1), APL should continue to copy whatever KCs do. Thus, APL odor responses should increase after adaptation just as KC odor responses do. Contrary to this prediction, after 4 d at 31 °C, APL>dTRPA,GCaMP6f flies showed decreased APL odor responses compared with APL>GCaMP6f (no dTRPA1) flies (Fig. 4*C*), particularly in the peak response (compare with steady-state responses in *SI Appendix*, Fig. S13). These results suggest that increased KC odor responses after adaptation can be explained at least in part by

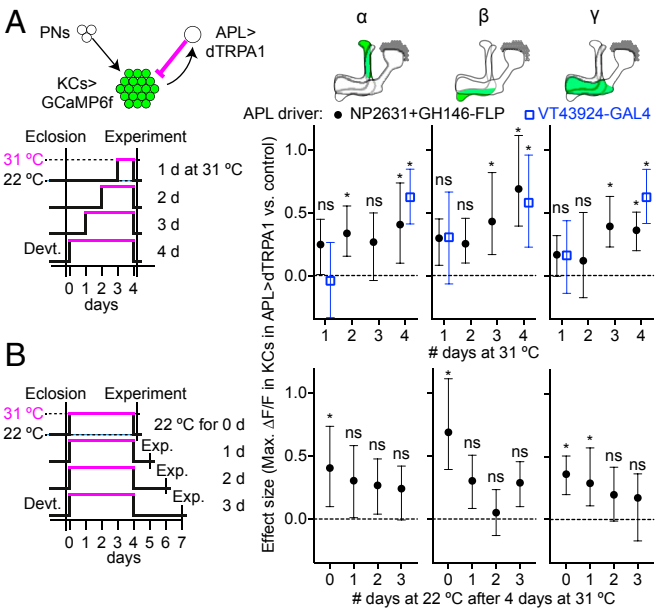

Fig. 3. Adaptation to excess inhibition from APL is most prominent after 4 d and is temporary. (*A*) Adaptation after 1, 2, 3, or 4 d of APL activation. Flies were raised at 22 °C and collected 0 to 1 d after eclosion, then kept at 22 °C for 0 to 3 d, then kept at 31 °C for 1 to 4 d, and imaged at 22 °C at 4 to 5 d posteclosion. Graphs show effect size of adaptation (maximum Δ*F*/*F* of KC response to isoamyl acetate, APL>dTRPA1 minus control), calculated using bootstrap-coupled estimation statistics (84), driving dTRPA1 expression in APL using NP2631+GH146-FLP (black circles; control is APL unlabeled) or VT43924-GAL4 (blue squares; control is UAS-dTRPA1/+). Error bars indicate 95% CIs. In the diagram of the genotype (*Upper Left*), green shows GCaMP6f expression, and magenta shows activation with dTRPA1. **P* < 0.05 for APL>dTRPA1 vs. control, ANOVA (see *SI Appendix*, Table S2 for details). ns (not significant; *P* > 0.05) applies to both drivers at 1 d. Full data and sample sizes for all lobes are in *SI Appendix*, Figs. S9–S11. (*B*) As in *A*, except flies were all kept at 31 °C for 4 d, and then kept at 22 °C for 0 to 3 d before imaging. Data for 0 d are repeated from "4 d" in *A* for comparison. Full data are in *SI Appendix*, Fig. S12.

decreased activity in the inhibitory APL neuron (mechanisms 3 and/or 4).

Different KCs Show Different Effects of APL Activation after Adaptation. These results do not rule out the possibility that, in addition to changes in APL activity, adaptation also involves changes centered on KC activity (mechanisms 1, 2, and 5 above: increased intrinsic excitability, increased synaptic excitation from PNs, and decreased sensitivity to inhibition from APL). To test this possibility, we reexamined data from *SI Appendix*, Fig. S6 to focus on KC odor responses during acute activation of APL (caused by heating APL>dTRPA1 flies to 31 °C during imaging) (Fig. 5 *C* and *D*). Artificially activating APL overrules the reduced odor-evoked activity in APL, making APL activity equal in adapted and nonadapted flies, both before and during odor pulses (Fig. 5 *A* and *B* and *SI Appendix*, Fig. S14). Therefore, if adaptation was due only to reduced APL odor-evoked activity, then the difference in KC odor response between adapted and nonadapted flies should go away when we artificially activate APL.

We observed different results in different KCs. In αβ KCs, odor responses in adapted flies were generally still higher than in nonadapted flies even at 31 °C (Fig. 5*E*). In contrast, in γ KCs, although odor responses were higher in adapted than nonadapted flies when recorded at 22 °C, the odor responses declined approximately to the same level when recorded at 31 °C (Fig. 5*E*). (Note that Fig. 5 shows mean Δ*F*/*F* rather than maximum Δ*F*/F because in some cases activating APL with dTRPA1 changed the dynamics of the KC odor responses; see *SI Appendix*, Fig. S15 for maximum Δ*F*/*F*, which gives similar results.) A power analysis indicates our sample sizes would detect an effect as strong as that observed in the β lobe with power >0.95. (Odor responses in α′β′ KCs are more difficult to interpret as they did not consistently decrease when APL was activated by dTRPA1; *SI Appendix*, Figs. S6, S7, and S15.) These results indicate that while adaptation in γ KCs can be explained by decreased APL odor responses, adaptation in αβ KCs requires an additional mechanism.

Adaptation in αβ KCs Occurs at Least Partly through Noninhibitory Plasticity. This additional mechanism in αβ KCs could be mechanisms 1, 2, and/or 5: increased intrinsic excitability, increased synaptic excitation from PNs, and/or decreased sensitivity to inhibition from APL. To distinguish between these possibilities (Fig. 6*A*), we sought to block inhibition from APL in adapted flies (Fig. 6*B*). If adaptation occurred solely through weakening inhibition, whether through reducing APL activity (mechanisms 3 and 4) or reducing KC sensitivity to inhibition (mechanism 5), then blocking inhibition should remove the difference between adapted and nonadapted flies. To acutely block inhibition from

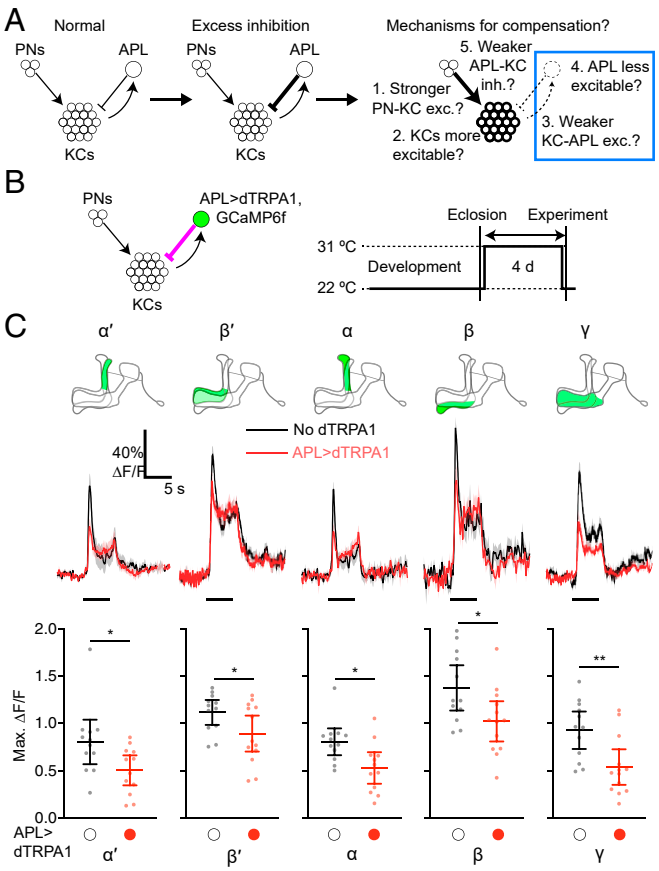

Fig. 4. APL odor responses are reduced following adaptation. (*A*) Diagrams of potential mechanisms that might underlie increased KC odor responses following adaptation. This figure tests mechanisms 1, 2, and 5 vs. mechanisms 3 and 4, and shows evidence for mechanisms 3 and 4 (blue box). (*B*) Diagram of genotype (APL expresses dTRPA1 and GCaMP6f) and experimental protocol (all flies were raised at 22 °C and kept at 31 °C for 4 d before imaging). (*C*) Responses of different lobes of APL (as determined by the anatomical marker MB247-dsRed) to isoamyl acetate in APL>GCaMP6f ("No dTRPA1") or APL>dTRPA1,GCaMP6f ("APL>dTRPA1") flies kept at 31 °C for 4 d. Diagrams show the locations of different lobes (green) within APL, which innervates the whole mushroom body. Graphs show maximum Δ*F*/*F* and mean ± 95% CIs; shading indicates SEM. **P* < 0.05, ***P* < 0.01, unpaired *t* test or Mann–Whitney *U* test (see *SI Appendix*, Table S2 for details). *n*, given as the number of hemispheres (number of flies), left to right: α′ and α, 12 (9), 12 (8); β′, β, and γ, 12 (9), 13 (8).

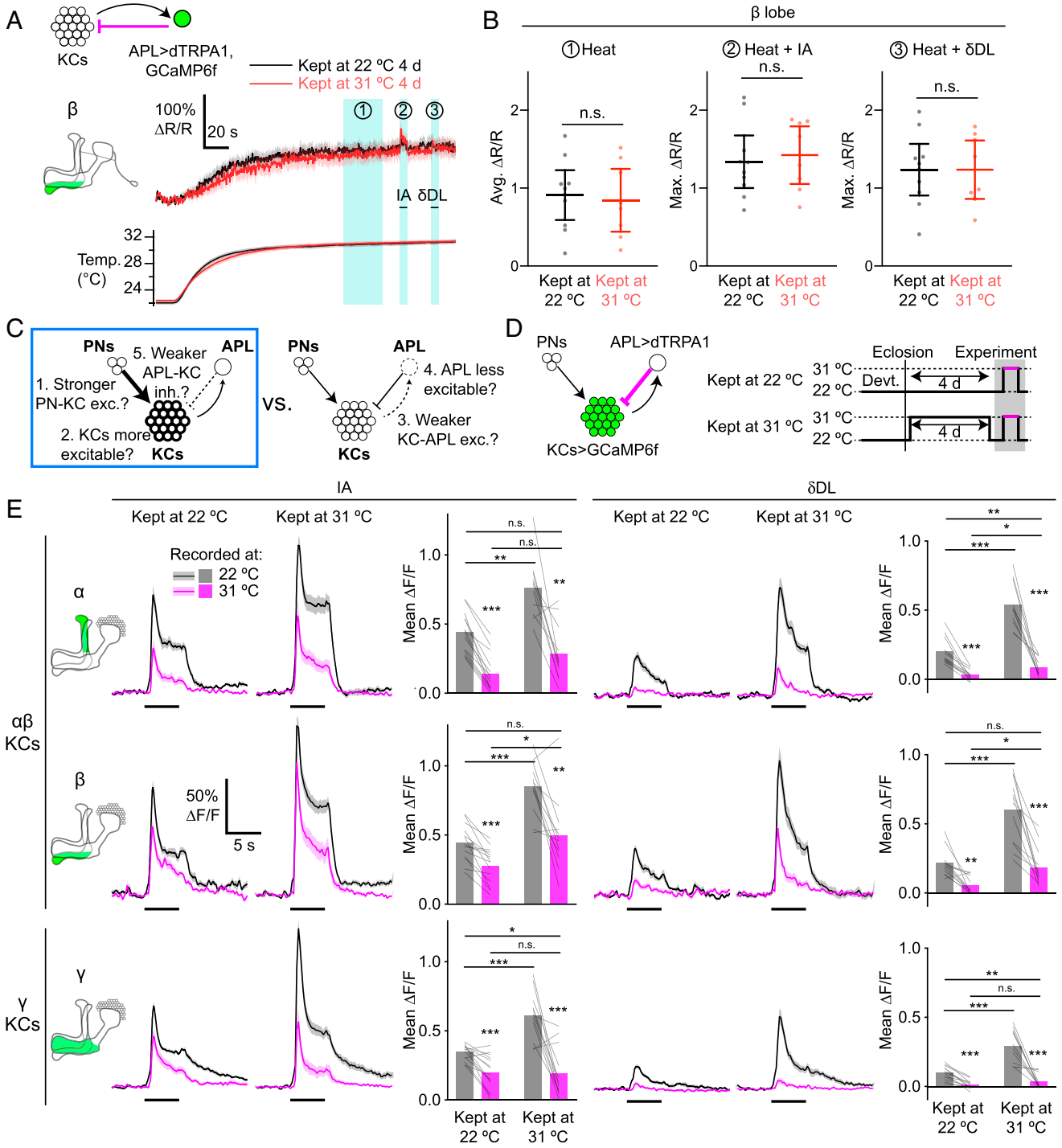

Fig. 5. Different KCs show different effects of APL activation after adaptation. (*A*) APL is equally activated by dTRPA1 regardless of preheating. (*A*, *Upper*) Traces show GCaMP6f signal of the β lobe of APL (as determined by the anatomical marker MB247-dsRed), normalized to dsRed signal (hence Δ*R*/*R*, not Δ*F*/*F*), during perfusion heating of saline, in APL>TRPA,GCaMP6f flies kept at 22 °C (black) or 31 °C (red) for 4 d. Blue shading shows periods used for quantification in *B*. After the temperature reached a plateau (period 1), isoamyl acetate (period 2) and δ-decalactone (period 3) were presented. (*A*, *Lower*) Traces show the saline temperature corresponding to recordings in the *Upper* traces (same color scheme and timescale). Shading indicates SEM. Other lobes are shown in *SI Appendix*, Fig. S14. (*B*) Quantification of periods from *A*: average Δ*R*/*R* during temperature plateau (period 1) and maximum Δ*R*/*R* during odors (periods 2 and 3). Maximum Δ*R*/*R* is used for odors for consistency with Fig. 4. Graphs show mean ± 95% CIs. n.s., $P > 0.05$, unpaired *t* test or Mann–Whitney *U* test. *n*, given as the number of hemispheres (number of flies), left to right: 22 °C, 10 (8); 31 °C, 8 (6). (*C*) This figure tests mechanisms 1, 2, and 5 vs. mechanisms 3 and 4, and shows evidence for mechanisms 1, 2, and 5 (blue box) in αβ KCs. (*D*) Diagram of genotype (APL expresses dTRPA1; KCs express GCaMP6f) and experimental protocol for *E*. (*E*) Traces show responses of the α, β, and γ lobes to isoamyl acetate (*Left*) and δ-decalactone (*Right*) in KC>GCaMP6f and APL>dTRPA1 flies kept at 22 or 31 °C for 4 d, recorded at 22 °C (black) or 31 °C (magenta). Only paired recordings are shown (the same fly is recorded at both temperatures). Black bars indicate 5-s odor pulse; shading indicates SEM. Bar graphs quantify traces using mean Δ*F*/*F* during the odor pulse (the same color scheme as the traces; bars show the mean; thin lines show paired data recorded at 22 and 31 °C). Data for α′β′ KCs and maximum Δ*F*/*F* are given in *SI Appendix*, Fig. S15. *$P <$ 0.05, **$P < 0.01$, ***$P < 0.001$, paired *t* test or Wilcoxon test (22 vs. 31 °C), unpaired *t* test or Mann–Whitney *U* test (across flies), with Holm–Bonferroni correction (see *SI Appendix*, Table S2 for details). *n* are as in *SI Appendix*, Figs. S6 and S7.

APL in preheated APL>dTRPA1 flies, we expressed the histamine-gated Cl^- channel Ort (53) in APL and bath applied histamine. Ectopically expressing Ort in olfactory neurons allows histamine to potently inhibit them for at least several minutes (54). We again used the intersectional driver for APL to express dTRPA1 and Ort in APL, and MB247-LexA to express GCaMP6f in KCs. In hemispheres where APL was unlabeled, 2 mM histamine did not affect KC odor responses (Fig. 6*C* and *SI Appendix*, Fig. S16); this result is consistent with the relative absence of histamine and histamine receptors in the mushroom body (54–60), and argues against non-specific effects of histamine.

In Figs. 2 and 3, the adapted vs. nonadapted conditions were hemispheres in APL>dTRPA1 flies where APL was labeled or unlabeled, respectively. However, in this experiment, we could not use APL unlabeled hemispheres as controls, because here we sought to compare adapted vs. nonadapted flies when APL was blocked by Ort, which is not expressed if APL is unlabeled. In theory, the nonadapted controls could be either APL>dTRPA1,Ort flies kept at 22 °C or APL>Ort flies (without dTRPA1) kept at 31 °C. However, in preliminary experiments, we found that in APL>dTRPA1,Ort flies kept at 22 °C for 4 d, histamine increased KC odor responses modestly but not as strongly as in APL>dTRPA1,Ort or APL>Ort flies kept at 31 °C for 4 d (*SI Appendix*, Fig. S16). This temperature dependence suggests that Ort expression was stronger at 31 than 22 °C because Gal4 activity is stronger at higher temperatures (61). Therefore, APL>dTRPA1,Ort flies kept at 22 °C were not a suitable control. Instead, we compared only flies kept at 31 °C for 4 d: APL>dTRPA1,Ort (adapted) and APL>Ort (nonadapted).

These genotypes replicated the adaptation effect: Before adding histamine, responses in APL>dTRPA1,Ort hemispheres were higher than responses in APL>Ort (no dTRPA1) hemispheres. (In the α′ and β′ lobes, this difference was not statistically significant [*SI Appendix*, Fig. S17]; it may be that any adaptation effect in α′β′ KCs is less robust than in αβ and γ KCs, as in *SI Appendix*, Figs. S4, S9, S11, and S12.) After adding histamine, KC responses in both genotypes were dramatically increased, to a similar degree as that caused by tetanus toxin expression in APL (*SI Appendix*, Fig. S18), suggesting that in flies kept at 31 °C, stimulating Ort in APL with 2 mM histamine suffices to block APL inhibition onto KCs.

In the α and β lobes, after adding histamine, responses to isoamyl acetate in APL>dTRPA1,Ort hemispheres were still significantly higher than in APL>Ort hemispheres (Fig. 6 *C* and *D*). That is, even without inhibition from APL, we still observed the adaptation effect, suggesting that the adaptation from excess APL inhibition occurs at least in part through noninhibitory plasticity, namely increased synaptic excitation or intrinsic excitability (mechanism 1 or 2), rather than entirely through decreased sensitivity to inhibition or decreased activity in APL (mechanisms 3 to 5). In contrast, in the γ lobe, although APL>dTRPA1,Ort responses were slightly higher than APL>Ort responses after adding histamine, this difference was not statistically different. This result suggests that in γ KCs, adaptation from excess APL inhibition mostly relies on reduced inhibition (mechanisms 3 to 5). Note that we do not exclude the possibility that APL>dTRPA1,Ort and APL>Ort γ-lobe responses were actually different and we lacked the statistical power to detect a significant effect due to experimental variability. Still, this difference between αβ and γ KCs is consistent with the conclusion from APL activation during imaging (Fig. 5) that adaptation in γ KCs can be explained mostly by decreased APL activity (mechanisms 3 and 4) while adaptation in αβ KCs requires something extra.

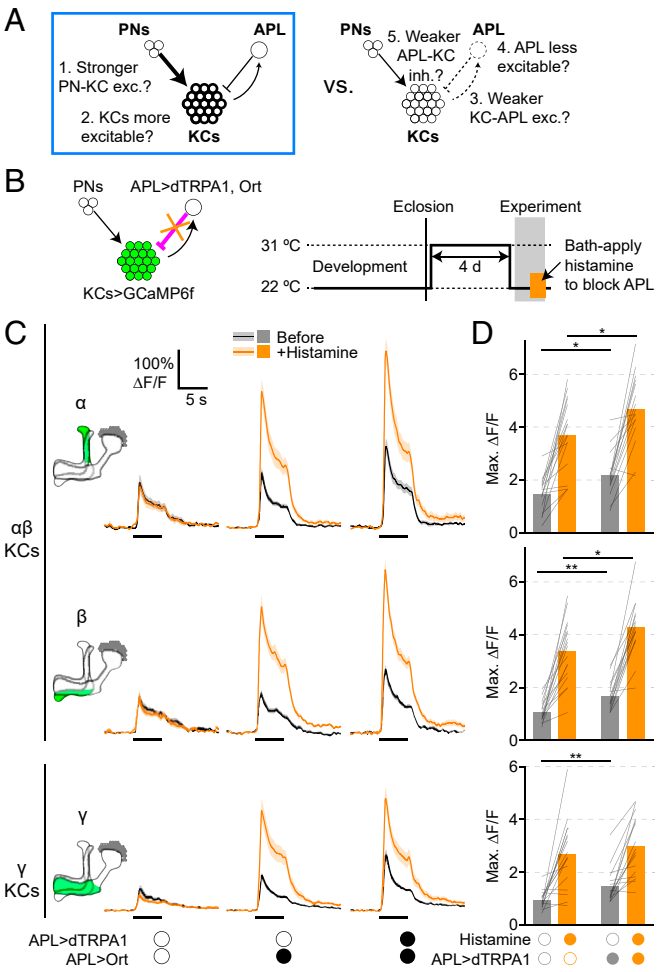

Fig. 6. Adaptation effect remains in αβ KCs after removing inhibition from APL. (*A*) This figure tests mechanisms 1 and 2 vs. mechanisms 3 to 5, and shows evidence for mechanisms 1 and 2 (blue box) in αβ KCs. (*B*) Diagram of genotype and experimental protocol. Flies were raised at 22 °C, collected 0 to 1 d after eclosion, kept at 31 °C for 4 d, and returned to 22 °C for the imaging experiment. During the experiment, odor responses were recorded before and after bath applying 2 mM histamine. (*C*) Responses of α, β, and γ lobes to isoamyl acetate before (black) and after (orange) bath applying 2 mM histamine. Genotypes: mixture of hemispheres from APL>Ort and APL>dTRPA1,Ort flies where APL was unlabeled (*Left*), APL>Ort, APL labeled (*Center*), and APL>dTRPA1,Ort, APL labeled (*Right*). Shading indicates SEM. Traces of other lobes and responses to δ-decalactone are shown in *SI Appendix*, Figs. S16 and S17. (*D*) Maximum Δ*F*/*F* for traces in *C*. Genotypes: APL>Ort (*Left*), APL>dTRPA1,Ort (*Right*). Bars show mean; thin lines show paired data (same hemisphere before and after histamine). The effect of histamine was statistically significant in all cases ($P < 0.001$, paired *t* test or Wilcoxon test). **P* < 0.05, ***P* < 0.01, unpaired *t* test or Mann–Whitney *U* test, Holm–Bonferroni correction for multiple comparisons (see *SI Appendix*, Table S2 for details). *n*, given as the number of hemispheres (number of flies), left to right: no dTRPA1, 17 (11); APL>dTRPA1, 16 (11).

Discussion

We have delineated the homeostatic capacity of the *Drosophila* mushroom body in vivo and revealed circuit mechanisms underlying homeostatic plasticity. We found that the mushroom body compensates for excess inhibition from APL, but not lack of inhibition. This compensation requires multiple days and occurs by two mechanisms—suppressed odor-evoked APL activity and increased odor-evoked excitation of KCs—which contribute differentially to adaptation in different subtypes of KCs.

We did not observe clear evidence of compensation for lack of inhibition in APL>TNT flies. Could this be because our acute manipulation (16- to 24-h TNT expression in APL) was already long enough to induce adaptation? Two lines of evidence argue against this possibility. First, the effect of blocking APL with 16 to 24 h of TNT expression is at least as strong as the effect of

blocking APL with shibire^{ts}, which occurs over only ~15 min (1). Second, we saw similar size effects for 16- to 24-h APL>TNT expression and APL>Ort + 5-min histamine bath application (*SI Appendix*, Fig. S18). Because 16- to 24-h APL>TNT expression produces a similar effect on KCs as two separate acute blockades of APL, we consider it unlikely that a shorter TNT blockade would produce larger KC odor responses.

Why do KCs show little compensation for lack of inhibition in APL>TNT flies? For example, KCs could in theory increase expression of potassium channels to reduce their excitability (45), yet apparently they do not. It may be that the mushroom body normally tries to compensate for increased KC activity by increasing inhibition from APL (i.e., mechanisms 3 to 5 in the scheme in Fig. 4*A*, but in the opposite direction), but this strategy fails in APL>TNT flies because synaptic output from APL is permanently blocked. (Indeed, we observed anecdotally that prolonged APL>TNT expression appeared to make APL's neurites degenerate; *SI Appendix*, Fig. S19.) This explanation would be consistent with findings in mammals that hyperexcitability is compensated for by increased synaptic inhibition (62–64). Such mechanisms would successfully adapt for variable APL activity; their only failure mode (complete inactivation of APL) might be rare enough not to be worth evolving compensation for. The lack of compensation for blockade of APL may not be surprising in light of other findings that even strong homeostatic compensation can be imperfect (65).

We imposed excess inhibition on KCs by activating APL with dTRPA1 for 4 d. Although it was not technically feasible to verify by in vivo recordings that APL was continuously activated throughout the 4 d, Fig. 5*A* and *SI Appendix*, Fig. S14 show that 1) dTRPA1 activation drives Ca^{2+} influx in APL to a plateau lasting as long as an ~3- to 4-min heat stimulus, and 2) APL activation during imaging is not affected by APL preactivation for 4 d. APL is unlikely to enter depolarization block as it does not fire action potentials (66). Similarly, activating APL with dTRPA1 still suppresses KC odor responses after a 4-d preactivation (Fig. 4 and *SI Appendix*, Figs. S6 and S7). These results suggest that APL most likely was depolarized throughout the 4-d preactivation.

What mechanisms underlie the observed compensation for excess inhibition from APL? We initially postulated five nonmutually exclusive categories of mechanisms: 1) increased synaptic excitation from PNs to KCs, 2) increased intrinsic excitability of KCs, 3) decreased synaptic excitation from KCs to APL, 4) decreased intrinsic excitability of APL, and 5) decreased synaptic inhibition from APL to KCs (Fig. 4*A*). Our finding that APL shows decreased odor responses after adaptation (Fig. 4) implicates decreased synaptic excitation and/or intrinsic excitability of APL (mechanisms 3 and 4). The equal activation of APL by dTRPA1 in control vs. adapted flies (Fig. 5*A*) might argue against decreased intrinsic excitability of APL. However, dTRPA1 activation might be so strong as to cause a ceiling effect, or GAL4-driven dTRPA1 expression in APL might be higher in preheated flies (61), cancelling out any decreased intrinsic excitability.

Our finding of decreased APL activity after APL overactivation is consistent with previous studies showing the converse result, that mammalian interneurons increase their excitability when their activity is blocked (67–69). Yet other studies found opposite effects: Decreasing network activity decreases excitability of interneurons while increasing activity increases it (10, 21, 23, 51). These differences likely arise from whether the system's homeostatic set point focuses on single neurons (i.e., inhibitory interneurons try to maintain their desired activity) or the network as a whole (i.e., if total network activity is decreased, even including decreased interneuron activity, interneurons should still decrease their excitability to disinhibit the network) (70). In our case, both scenarios point in the same direction, as our manipulation activates an inhibitory interneuron (APL) that then inhibits the principal excitatory neurons (KCs); both the primary and secondary effects demand decreased APL excitability as the correct homeostatic response.

We further found that αβ (but not γ) KCs continue to show the adaptation effect when APL is artificially activated (Fig. 5) or blocked (Fig. 6), implicating increased synaptic excitation or intrinsic excitability of KCs (mechanisms 1 and/or 2 in αβ KCs). These findings are consistent with other studies showing increased excitation/excitability of excitatory neurons in response to decreased activity (7, 12, 19, 52, 71, 72). Note that we do not exclude the possibility of decreased synaptic inhibition from APL to KCs (mechanism 5); such weakening of inhibition onto excitatory neurons commonly occurs in response to neuronal inactivity (7, 8, 11, 73). Finally, in contrasting αβ KCs and γ KCs, we do not claim that γ KCs show absolutely no changes in excitation, merely that we did not find evidence of such changes.

What molecular mechanisms may be involved? Neurons in the circuit might sense their abnormally high (APL) or low (KC) activity by reactive oxygen species via the redox sensor DJ-1β (29) or by Ca^{2+} levels via CaM kinase (9, 72). Our finding that adaptation takes more than 1 d suggests that the effector arm of the homeostatic mechanism may involve altered transcription or translation. Increased (KCs) or decreased (APL) synaptic excitation (mechanisms 1 and 3 above) might occur through altered synapse size/number (30) or altered surface expression of postsynaptic nicotinic acetylcholine receptors, as occurs with α-amino-3-hydroxy-5-methyl-4-isoxazolepropionic acid (AMPA) receptors in plasticity of glutamatergic synapses (74, 75). Such changes could also occur by altered presynaptic release from PNs or KCs, respectively. However, we consider presynaptic plasticity in PNs less likely, as this would be expected to affect all KCs equally rather than only αβ KCs, whereas we only observed increased excitation/excitability in αβ KCs, not γ KCs. Increased (KCs) or decreased (APL) intrinsic excitability (mechanisms 2 and 4 above) might occur through altered ion channel expression, as observed in *Drosophila* larval motor neurons (32), or (for KCs) through moving the axon initial segment (76, 77).

We do not exclude the possibility that other neurons in the mushroom body could be involved in the observed homeostatic compensation. For example, the DPM (dorsal paired medial) neuron also forms reciprocal synapses with KCs (78) and contains γ-aminobutyric acid (GABA) (79), so it may be that DPM reduces inhibition of KCs to compensate for excess inhibition from APL. However, unlike APL, DPM shows little or no expression of GABAergic markers (56). Moreover, there is no published physiological evidence that DPM directly inhibits KCs; DPM and APL are connected by gap junctions (80), so findings that activating DPM increases chloride concentrations in KCs (79) could be explained by DPM activating APL. If increased KC activity arises in part from decreased DPM activity causing decreased APL activity via DPM–APL gap junctions, this could be considered a special case of decreased synaptic excitation from KCs to APL.

Our findings that adaptation occurs over multiple days (Fig. 3 and *SI Appendix*, Figs. S9–S11) fit in with diverse adaptation timescales in other in vivo studies. Following sensory deprivation in mammals, recovery of cortical activity levels from their nadir can take ~1 to 3 d (21, 48, 81), even up to 7 d (24). In other cases, adaptation occurs within 24 h (19, 23, 50, 51). It may be that the incomplete suppression of KC odor responses by APL>dTRPA1 activation (Fig. 5 and *SI Appendix*, Figs. S6 and S7) is a less drastic effect than, for example, the effect of eyelid suture on visually evoked cortical activity. Intuitively, it is reasonable that homeostatic mechanisms may take longer to sense and respond to a less drastic activity perturbation. Alternatively, it may simply be that the mushroom body is less efficient at compensating for activity perturbations than the mammalian cortex, whether due

to differences between species or types of brain structures. Future studies may address these and other questions about the timescale of adaptation, such as whether adaptation occurs in older flies, or whether different underlying mechanisms kick in at different times during the multiday unfolding of homeostatic adaptation.

Finally, what is the behavioral significance of homeostatic adaptation in Kenyon cells? In the example studied here, increased KC activity following excess inhibition makes odor responses less sparse (Fig. 2 *D*), which could impair learned odor discrimination (1). However, it is unclear if the relatively modest decrease in sparseness would measurably impair odor discrimination, especially as we did not detect a significant increase in interodor correlations. Indeed, the adaptation might even improve associative olfactory learning, given that improved learning is seen when KC activity is modestly increased by down-regulating GABA synthesis in APL (vs. blocking APL output completely) (1, 36, 37). Future work may address which (if any) of these potential behavioral outcomes occurs. Conversely, given that homeostatic compensation following APL>dTRPA1 preactivation allows odor responses of αβ (but not γ) KCs to approach normal amplitudes during acute APL>dTRPA1 activation despite the excess inhibition (Fig. 5), it will be interesting to test whether preactivating APL analogously allows flies to resist whatever learning impairment (if any) might normally result from acutely inhibiting KCs with APL>dTRPA1. If so, homeostatic adaptation might help flies avoid detection failures in the case of hyperinhibition. Indeed, a greater need to avoid detection failures than discrimination failures could explain why the mushroom body compensates for KC hypoactivity but not hyperactivity. More generally, homeostatic plasticity may reflect broader activity-dependent parameter setting in KCs that helps achieve reliably distributed sparse odor coding (82).

Methods

See *SI Appendix, Methods* for details.

Fly Strains. Flies were raised on standard cornmeal agar at the temperatures described. Details of fly strains are given in *SI Appendix, Methods*.

Imaging. Brains were imaged by two-photon microscopy on a Movable Objective Microscope (Sutter) using ScanImage software (Vidrio), as described (1, 43). Volume imaging was performed in sawtooth mode (typically 10 to 16 *z* slices, volume rate ∼3 Hz). Movies were motion-corrected in *X*–*Y* using the moco ImageJ plugin (83), and motion-corrected in *Z* by maximizing the pixel-by-pixel correlation between each volume and the average volume across time points (43). Δ*F*/*F* traces were calculated in ImageJ using manually drawn regions of interest for the background and brain structure of interest, and smoothed with a 0.2-s boxcar filter and interpolated to common frame times for averaging traces in Igor Pro 7 (WaveMetrics). Δ*R*/*R* in Fig. 5 and *SI Appendix*, Fig. S14 was calculated by dividing GCaMP6f signal by dsRed signal, to remove motion artifacts caused by heating. Sparseness and correlation were analyzed as in ref. 1. Histamine (2 mM; Sigma; H7250) was added 5 min before imaging in APL>Ort experiments.

Data Availability. All data necessary to reproduce our findings and figures are included in Dataset S1. Analysis code is available on GitHub at https://github.com/aclinlab/calcium-imaging.

ACKNOWLEDGMENTS. We thank members of the A.C.L. and Juusola laboratories for discussions; Moshe Parnas, Mikko Juusola, and Anton Nikolaev for comments on the manuscript; Lily Bolsover, Chloe Donahue, Kath Whitley, Josh Marston, Rachael Thomas, and Rachid Achour for technical assistance; and Chi-hon Lee (Academia Sinica), the Bloomington Stock Center, and the Vienna *Drosophila* Resource Center for flies. This work was supported by the European Research Council (project no. 639489) and the Biotechnology and Biological Sciences Research Council (project no. BB/S016031/1).

1. A. C. Lin, A. M. Bygrave, A. de Calignon, T. Lee, G. Miesenböck, Sparse, decorrelated odor coding in the mushroom body enhances learned odor discrimination. *Nat. Neurosci.* **17**, 559–568 (2014).
2. B. A. Olshausen, D. J. Field, Sparse coding of sensory inputs. *Curr. Opin. Neurobiol.* **14**, 481–487 (2004).
3. A. Litwin-Kumar, B. Doiron, Formation and maintenance of neuronal assemblies through synaptic plasticity. *Nat. Commun.* **5**, 5319 (2014).
4. T. O'Leary, A. H. Williams, A. Franci, E. Marder, Cell types, network homeostasis, and pathological compensation from a biologically plausible ion channel expression model. *Neuron* **82**, 809–821 (2014). Correction in: *Neuron* **88**, 1308 (2015).
5. T. Keck, M. Hübener, T. Bonhoeffer, Interactions between synaptic homeostatic mechanisms: An attempt to reconcile BCM theory, synaptic scaling, and changing excitation/inhibition balance. *Curr. Opin. Neurobiol.* **43**, 87–93 (2017).
6. G. Turrigiano, Too many cooks? Intrinsic and synaptic homeostatic mechanisms in cortical circuit refinement. *Annu. Rev. Neurosci.* **34**, 89–103 (2011).
7. A. Maffei, S. B. Nelson, G. G. Turrigiano, Selective reconfiguration of layer 4 visual cortical circuitry by visual deprivation. *Nat. Neurosci.* **7**, 1353–1359 (2004).
8. A. Maffei, G. G. Turrigiano, Multiple modes of network homeostasis in visual cortical layer 2/3. *J. Neurosci.* **28**, 4377–4384 (2008).
9. C. P. Goold, R. A. Nicoll, Single-cell optogenetic excitation drives homeostatic synaptic depression. *Neuron* **68**, 512–528 (2010).
10. M. C. Chang *et al*., Narp regulates homeostatic scaling of excitatory synapses on parvalbumin-expressing interneurons. *Nat. Neurosci.* **13**, 1090–1097 (2010).
11. C. G. Lau, V. N. Murthy, Activity-dependent regulation of inhibition via GAD67. *J. Neurosci.* **32**, 8521–8531 (2012).
12. N. S. Desai, R. H. Cudmore, S. B. Nelson, G. G. Turrigiano, Critical periods for experience-dependent synaptic scaling in visual cortex. *Nat. Neurosci.* **5**, 783–789 (2002).
13. P. Wenner, Homeostatic synaptic plasticity in developing spinal networks driven by excitatory GABAergic currents. *Neuropharmacology* **78**, 55–62 (2014).
14. A. Destexhe, M. Rudolph, D. Paré, The high-conductance state of neocortical neurons in vivo. *Nat. Rev. Neurosci.* **4**, 739–751 (2003).
15. S. A. Kirov, K. E. Sorra, K. M. Harris, Slices have more synapses than perfusion-fixed hippocampus from both young and mature rats. *J. Neurosci.* **19**, 2876–2886 (1999).
16. B. N. Cazakoff, B. Y. B. Lau, K. L. Crump, H. S. Demmer, S. D. Shea, Broadly tuned and respiration-independent inhibition in the olfactory bulb of awake mice. *Nat. Neurosci.* **17**, 569–576 (2014).
17. L. D. Knogler, M. Liao, P. Drapeau, Synaptic scaling and the development of a motor network. *J. Neurosci.* **30**, 8871–8881 (2010).
18. R. Mongeon *et al*., Synaptic homeostasis in a zebrafish glial glycine transporter mutant. *J. Neurophysiol.* **100**, 1716–1723 (2008).
19. T. Keck *et al*., Synaptic scaling and homeostatic plasticity in the mouse visual cortex in vivo. *Neuron* **80**, 327–334 (2013).
20. S. J. Barnes *et al*., Subnetwork-specific homeostatic plasticity in mouse visual cortex in vivo. *Neuron* **86**, 1290–1303 (2015).
21. K. B. Hengen, M. E. Lambo, S. D. Van Hooser, D. B. Katz, G. G. Turrigiano, Firing rate homeostasis in visual cortex of freely behaving rodents. *Neuron* **80**, 335–342 (2013).
22. K. B. Hengen, A. Torrado Pacheco, J. N. McGregor, S. D. Van Hooser, G. G. Turrigiano, Neuronal firing rate homeostasis is inhibited by sleep and promoted by wake. *Cell* **165**, 180–191 (2016).
23. S. J. Kuhlman *et al*., A disinhibitory microcircuit initiates critical-period plasticity in the visual cortex. *Nature* **501**, 543–546 (2013).
24. S. D. Greenhill, A. Ranson, K. Fox, Hebbian and homeostatic plasticity mechanisms in regular spiking and intrinsic bursting cells of cortical layer 5. *Neuron* **88**, 539–552 (2015).
25. H. Amin, A. C. Lin, Neuronal mechanisms underlying innate and learned olfactory processing in *Drosophila*. *Curr. Opin. Insect Sci.* **36**, 9–17 (2019).
26. J. M. Devaud, A. Acebes, A. Ferrús, Odor exposure causes central adaptation and morphological changes in selected olfactory glomeruli in *Drosophila*. *J. Neurosci.* **21**, 6274–6282 (2001).
27. S. Sachse *et al*., Activity-dependent plasticity in an olfactory circuit. *Neuron* **56**, 838–850 (2007).
28. S. Das *et al*., Plasticity of local GABAergic interneurons drives olfactory habituation. *Proc. Natl. Acad. Sci. U.S.A.* **108**, E646–E654 (2011).
29. M. C. Oswald *et al*., Reactive oxygen species regulate activity-dependent neuronal plasticity in *Drosophila*. *eLife* **7**, e39393 (2018).
30. M. C. Kremer *et al*., Structural long-term changes at mushroom body input synapses. *Curr. Biol.* **20**, 1938–1944 (2010).
31. C. A. Doll, D. J. Vita, K. Broadie, Fragile X mental retardation protein requirements in activity-dependent critical period neural circuit refinement. *Curr. Biol.* **27**, 2318–2330.e3 (2017).
32. C. J. Mee, E. C. G. Pym, K. G. Moffat, R. A. Baines, Regulation of neuronal excitability through Pumilio-dependent control of a sodium channel gene. *J. Neurosci.* **24**, 8695–8703 (2004).
33. G. W. Davis, Homeostatic signaling and the stabilization of neural function. *Neuron* **80**, 718–728 (2013).
34. H. Kazama, R. I. Wilson, Homeostatic matching and nonlinear amplification at identified central synapses. *Neuron* **58**, 401–413 (2008).
35. E. Gruntman, G. C. Turner, Integration of the olfactory code across dendritic claws of single mushroom body neurons. *Nat. Neurosci.* **16**, 1821–1829 (2013).
36. X. Liu, R. L. Davis, The GABAergic anterior paired lateral neuron suppresses and is suppressed by olfactory learning. *Nat. Neurosci.* **12**, 53–59 (2009).

37. Z. Lei, K. Chen, H. Li, H. Liu, A. Guo, The GABA system regulates the sparse coding of odors in the mushroom bodies of *Drosophila*. *Biochem. Biophys. Res. Commun.* **436**, 35–40 (2013).
38. K. S. Honegger, R. A. A. Campbell, G. C. Turner, Cellular-resolution population imaging reveals robust sparse coding in the *Drosophila* mushroom body. *J. Neurosci.* **31**, 11772–11785 (2011).
39. A. M. Mittal, D. Gupta, A. Singh, A. C. Lin, N. Gupta, Multiple network properties overcome random connectivity to enable stereotypic sensory responses. *Nat. Commun.* **11**, 1023 (2020).
40. O. Mayseless *et al*., Developmental coordination during olfactory circuit remodeling in *Drosophila*. *Neuron* **99**, 1204–1215.e5 (2018).
41. J. L. Pitman *et al*., A pair of inhibitory neurons are required to sustain labile memory in the *Drosophila* mushroom body. *Curr. Biol.* **21**, 855–861 (2011).
42. E. A. Hallem, J. R. Carlson, Coding of odors by a receptor repertoire. *Cell* **125**, 143–160 (2006).
43. N. Bielopolski *et al*., Inhibitory muscarinic acetylcholine receptors enhance aversive olfactory learning in adult *Drosophila*. *eLife* **8**, e48264 (2019).
44. G. C. Turner, M. Bazhenov, G. Laurent, Olfactory representations by *Drosophila* mushroom body neurons. *J. Neurophysiol.* **99**, 734–746 (2008).
45. L. N. Groschner, L. Chan Wah Hak, R. Bogacz, S. DasGupta, G. Miesenböck, Dendritic integration of sensory evidence in perceptual decision-making. *Cell* **173**, 894–905 (2018).
46. K. Inada, Y. Tsuchimoto, H. Kazama, Origins of cell-type-specific olfactory processing in the *Drosophila* mushroom body circuit. *Neuron* **95**, 357–367.e4 (2017).
47. F. N. Hamada *et al*., An internal thermal sensor controlling temperature preference in *Drosophila*. *Nature* **454**, 217–220 (2008).
48. M. Y. Frenkel, M. F. Bear, How monocular deprivation shifts ocular dominance in visual cortex of young mice. *Neuron* **44**, 917–923 (2004).
49. C.-L. Wu, M.-F. M. Shih, P.-T. Lee, A.-S. Chiang, An octopamine-mushroom body circuit modulates the formation of anesthesia-resistant memory in *Drosophila*. *Curr. Biol.* **23**, 2346–2354 (2013).
50. S. J. Barnes *et al*., Deprivation-induced homeostatic spine scaling in vivo is localized to dendritic branches that have undergone recent spine loss. *Neuron* **96**, 871–882.e5 (2017).
51. M. A. Gainey, J. W. Aman, D. E. Feldman, Rapid disinhibition by adjustment of PV intrinsic excitability during whisker map plasticity in mouse S1. *J. Neurosci.* **38**, 4749–4761 (2018).
52. G. G. Turrigiano, K. R. Leslie, N. S. Desai, L. C. Rutherford, S. B. Nelson, Activity-dependent scaling of quantal amplitude in neocortical neurons. *Nature* **391**, 892–896 (1998).
53. A. Pantazis *et al*., Distinct roles for two histamine receptors (hclA and hclB) at the *Drosophila* photoreceptor synapse. *J. Neurosci.* **28**, 7250–7259 (2008).
54. W. W. Liu, R. I. Wilson, Transient and specific inactivation of *Drosophila* neurons in vivo using a native ligand-gated ion channel. *Curr. Biol.* **23**, 1202–1208 (2013).
55. I. Pollack, A. Hofbauer, Histamine-like immunoreactivity in the visual system and brain of *Drosophila melanogaster*. *Cell Tissue Res.* **266**, 391–398 (1991).
56. Y. Aso *et al*., Nitric oxide acts as a cotransmitter in a subset of dopaminergic neurons to diversify memory dynamics. *eLife* **8**, e49257 (2019).
57. V. Croset, C. D. Treiber, S. Waddell, Cellular diversity in the *Drosophila* midbrain revealed by single-cell transcriptomics. *eLife* **7**, e34550 (2018).
58. K. Davie *et al*., A single-cell transcriptome atlas of the aging *Drosophila* brain. *Cell* **174**, 982–998.e20 (2018).
59. M. M. Shih, F. P. Davis, G. L. Henry, J. Dubnau, Nuclear transcriptomes of the seven neuronal cell types that constitute the *Drosophila* mushroom bodies. *G3 (Bethesda)* **9**, 81–94 (2019).
60. A. Crocker, X.-J. Guan, C. T. Murphy, M. Murthy, Cell-type-specific transcriptome analysis in the *Drosophila* mushroom body reveals memory-related changes in gene expression. *Cell Rep.* **15**, 1580–1596 (2016).
61. J. B. Duffy, GAL4 system in *Drosophila*: A fly geneticist's Swiss army knife. *Genesis* **34**, 1–15 (2002).
62. S. Sim, S. Antolin, C. W. Lin, Y. Lin, C. Lois, Increased cell-intrinsic excitability induces synaptic changes in new neurons in the adult dentate gyrus that require Npas4. *J. Neurosci.* **33**, 7928–7940 (2013).
63. Y.-R. Peng *et al*., Postsynaptic spiking homeostatically induces cell-autonomous regulation of inhibitory inputs via retrograde signaling. *J. Neurosci.* **30**, 16220–16231 (2010).
64. M. Xue, B. V. Atallah, M. Scanziani, Equalizing excitation-inhibition ratios across visual cortical neurons. *Nature* **511**, 596–600 (2014).
65. M. A. Howard, J. L. R. Rubenstein, S. C. Baraban, Bidirectional homeostatic plasticity induced by interneuron cell death and transplantation in vivo. *Proc. Natl. Acad. Sci. U.S.A.* **111**, 492–497 (2014).
66. M. Papadopoulou, S. Cassenaer, T. Nowotny, G. Laurent, Normalization for sparse encoding of odors by a wide-field interneuron. *Science* **332**, 721–725 (2011).
67. A. F. Bartley, Z. J. Huang, K. M. Huber, J. R. Gibson, Differential activity-dependent, homeostatic plasticity of two neocortical inhibitory circuits. *J. Neurophysiol.* **100**, 1983–1994 (2008).
68. L. C. Rutherford, S. B. Nelson, G. G. Turrigiano, BDNF has opposite effects on the quantal amplitude of pyramidal neuron and interneuron excitatory synapses. *Neuron* **21**, 521–530 (1998).
69. N. S. Desai, L. C. Rutherford, G. G. Turrigiano, BDNF regulates the intrinsic excitability of cortical neurons. *Learn. Mem.* **6**, 284–291 (1999).
70. P. Wenner, Mechanisms of GABAergic homeostatic plasticity. *Neural Plast.* **2011**, 489470 (2011).
71. J. Burrone, M. O'Byrne, V. N. Murthy, Multiple forms of synaptic plasticity triggered by selective suppression of activity in individual neurons. *Nature* **420**, 414–418 (2002).
72. K. Ibata, Q. Sun, G. G. Turrigiano, Rapid synaptic scaling induced by changes in postsynaptic firing. *Neuron* **57**, 819–826 (2008).
73. K. N. Hartman, S. K. Pal, J. Burrone, V. N. Murthy, Activity-dependent regulation of inhibitory synaptic transmission in hippocampal neurons. *Nat. Neurosci.* **9**, 642–649 (2006).
74. V. Anggono, R. L. Huganir, Regulation of AMPA receptor trafficking and synaptic plasticity. *Curr. Opin. Neurobiol.* **22**, 461–469 (2012).
75. C. J. Wierenga, K. Ibata, G. G. Turrigiano, Postsynaptic expression of homeostatic plasticity at neocortical synapses. *J. Neurosci.* **25**, 2895–2905 (2005).
76. M. S. Grubb, J. Burrone, Activity-dependent relocation of the axon initial segment fine-tunes neuronal excitability. *Nature* **465**, 1070–1074 (2010).
77. S. Trunova, B. Baek, E. Giniger, Cdk5 regulates the size of an axon initial segment-like compartment in mushroom body neurons of the *Drosophila* central brain. *J. Neurosci.* **31**, 10451–10462 (2011).
78. S.-Y. Takemura *et al*., A connectome of a learning and memory center in the adult *Drosophila* brain. *eLife* **6**, e26975 (2017).
79. P. R. Haynes, B. L. Christmann, L. C. Griffith, A single pair of neurons links sleep to memory consolidation in *Drosophila melanogaster*. *eLife* **4**, e03868 (2015).
80. C.-L. Wu *et al*., Heterotypic gap junctions between two neurons in the *Drosophila* brain are critical for memory. *Curr. Biol.* **21**, 848–854 (2011).
81. M. Kaneko, D. Stellwagen, R. C. Malenka, M. P. Stryker, Tumor necrosis factor-α mediates one component of competitive, experience-dependent plasticity in developing visual cortex. *Neuron* **58**, 673–680 (2008).
82. S. X. Luo, R. Axel, L. F. Abbott, Generating sparse and selective third-order responses in the olfactory system of the fly. *Proc. Natl. Acad. Sci. U.S.A.* **107**, 10713–10718 (2010).
83. A. Dubbs, J. Guevara, R. Yuste, moco: Fast motion correction for calcium imaging. *Front. Neuroinform.* **10**, 6 (2016).
84. J. Ho, T. Tumkaya, S. Aryal, H. Choi, A. Claridge-Chang, Moving beyond *P* values: Data analysis with estimation graphics. *Nat. Methods* **16**, 565–566 (2019).